Phaseless Near Field Antenna Measurements from Two Surface Scans - Numerical and Experimental Investigations

Benjamin Fuchs, Michael Mattes, Sébastien Rondineau, Laurent Le Coq

Phaseless Near Field Antenna Measurements from Two Surface Scans - Numerical and Experimental Investigations

Benjamin Fuchs, *Senior Member, IEEE,* Michael Mattes, Sébastien Rondineau, *Senior Member, IEEE,* and Laurent Le Coq

***Abstract*— Phaseless near field measurements are an attractive solution to characterize antennas at reasonable costs, especially at high frequencies. The source reconstruction method is applied to compute the equivalent currents representing the antenna under test using two phaseless surface scans. The reconstruction of these equivalent currents uses recently proposed phase retrieval algorithms that mitigate some of the shortcomings of existing techniques with an automatic settings of the initial guess. In addition to be readily available and easy to be plugged in electromagnetic modeling tools, these routines exhibit good phase recovery performances and robustness with respect to noise, separation between scanning planes and near field sampling step. The proposed procedure is applied to determine the far field radiated by various types of antennas operating in different frequency bands from phaseless near field scans. Experimental validations of two radiating structures show its potentialities and interest.**

***Index Terms*— Antenna measurements, phaseless measurement, phase retrieval.**

I. Introduction

NEAR field antenna measurements require the acquisition of the field in both magnitude and phase in order to compute the far field, or the field at any distance, and thereby extract the desired antenna radiation parameters [1]–[3]. However, the accurate measurement of the phase is not always possible due to technical and/or economical reasons. Roughly speaking, phase measurements become more difficult and costly with increasing frequency. The probe positioning inacurracy, the variation of the temperature, the bending of the RF cables are all potential factors that make the acquisition of the phase unreliable. Phaseless, also called magnitude-only or intensity-only, measurements are then the only alternative to properly characterize the antenna.

A. Phaseless Antenna Measurement Techniques

Phaseless antenna measurement techniques can be divided into three categories, namely the four magnitudes techniques [4], [5], the indirect holography techniques [6], [7] and the two scans techniques [8]–[17], as detailed in the overview paper [3] where the advantages and drawbacks of each approach are also thoroughly discussed. The most widespread approach, chosen in this paper, is the two scans technique. It entails measuring the magnitude of the field radiated by the Antenna Under Test (AUT) on two (sufficiently separated) surfaces that are typically of planar, cylindrical or spherical shape. Unlike the four magnitudes and the indirect holography techniques, this approach requires no hardware modification or extra reference antenna. The main additionnal cost of the two scans technique is the computational processing to solve the non-linear inverse problem in order to retrieve the field phase distribution and derive reliable radiation patterns.

Manuscript received xx, 2018; revised xx, xx.

This work was supported in part by the European Union through the European Regional Development Fund (ERDF), and by the french region of Brittany, Ministry of Higher Education and Research, Rennes Métropole and Conseil Départemental 35, through the CPER Project SOPHIE / STIC & Ondes.

B. Fuchs and L. Le Coq are with the IETR / University of Rennes I, France. (e-mail: {benjamin.fuchs;laurent.le-coq}@univ-rennes1.fr). M. Mattes is with the Technical University of Denmark (e-mail: mmattes@elektro.dtu.dk). S. Rondineau is with the University of Brasília, Brazil (e-mail: sebastien@unb.br).

B. Phase Retrieval Algorithms

The implementation of a phaseless antenna measurement technique implies the resolution of a notoriously difficult mathematical problem known as Phase Retrieval (PR). The PR problem can be formulated as follows:

$$\text{find } \mathbf{x} \quad \text{subject to } |\mathbf{A}\mathbf{x}| = \mathbf{y} \tag{1}$$

where the vector $\mathbf{y} \in \mathbb{R}^m$ contains the m real and positive valued phaseless near field measurements, $\mathbf{A} \in \mathbb{C}^{m\times n}$ is the known sensing matrix and $\mathbf{x}$ is the complex signal of length n to be retrieved. In our phaseless antenna measurement scenario, the matrix $\mathbf{A}$ is a discretized free space Green function that links the sources $\mathbf{x}$ to the radiated field of magnitude $\mathbf{y}$. Since the phase information is not available, more observations m than unknowns n are required for solving (1).

In its original form, the PR problem is not convex and was solved using alternating projection methods starting from the pioneer works of Gerchberg-Saxton [18] and Fienup [19]. These approaches are also known as plane-to-plane backpropagation methods. They iteratively estimate the missing phases of the measurements $\tilde{\phi}$ and then solve the linear problem $\mathbf{A}\mathbf{x} = \mathbf{y}e^{j\tilde{\phi}}$. Many smart variants have later been adapted and applied successfully for antenna phaseless measurement problems [8]–[17]. They can be sensitive to the initial phase guess and their convergence may be slow.

During the last few years, the papers from Candès et al. [20], [21] have sparked a new interest in the phase retrieval problem. They show that lifting the PR problem to a higher dimensional

space enables the use of semidefinite programming:

$$|\mathbf{a}_i^*\mathbf{x}|^2 = \mathbf{x}^*\mathbf{a}_i\mathbf{a}_i^*\mathbf{x} = \mathrm{Tr}(\mathbf{a}_i\mathbf{a}_i^*\mathbf{x}\mathbf{x}^*) = \mathrm{Tr}(\mathbf{a}_i\mathbf{a}_i^*\mathbf{X})$$

where $\mathbf{x}^*$ is the conjugate transpose of $\mathbf{x}$ and $\mathbf{a}_i^*$ denotes the i-th row of $\mathbf{A}$. The magnitude measurements y_i^2 are then linear in the matrix $\mathbf{X} = \mathbf{x}\mathbf{x}^*$. These convex relaxations (e.g. PhaseLift [20], [21] and PhaseCut [22]) have a guaranteed convergence under specific conditions. Unfortunately, their prohibitive computational costs make them intractable for most real life applications.

More recently, a new line of convex relaxation has been proposed to efficiently solve PR problems while operating directly in the original signal space (see e.g. [23]–[25], [27], [28], [31], [32]). The idea is to relax the non-convex constraints $|\mathbf{a}_i^*\mathbf{x}| = y_i$ by the convex inequalities $|\mathbf{a}_i^*\mathbf{x}| \leq y_i$ and look for the vector $\mathbf{x}$ that is the most aligned with the vector $\hat{\mathbf{x}}$, an approximate guess of the solution. The so-called PhaseMax relaxation [24], [25] amounts to solve the convex problem:

$$\text{maximize } \mathrm{Re}\{\mathbf{x}^*\hat{\mathbf{x}}\} \text{ subject to } |\mathbf{a}_i^*\mathbf{x}| \leq y_i, \ \ i = 1, \ldots, m$$

where m is the number of measurement points. The objective forces the solution $\mathbf{x}$ to lie along the boundary of the constraint set. If all constraints are active, then we have recovered the solution to the original non-convex problem (1). A similar formulation has been recently proposed and successfully numerically validated for phaseless antenna characterization in [26].

In this paper, we use non-convex approaches combined with a proper initialization that solve a least-squares formulation of the PR problem [28], [30]–[32]. These new approaches enable to solve efficiently in an automatic fashion large scale phase retrieval problems such as antenna phaseless measurements. These algorithms are now readily available thanks to the general purpose phase retrieval library PhasePack [33]. Non-convex phase retrieval algorithms have been recently applied for phaseless antenna near field to far field transformation in [34], where the smart combination of probe signals enables to avoid suboptimal solutions. It has been successfully validated experimentally paving the way to efficient antenna phaseless measurement procedures.

C. Contributions and Outline

In this paper, the phaseless near field antenna measurement is formulated as a reconstruction of equivalent currents representing the AUT based on two field magnitude scans. This procedure is similar to the source reconstruction method presented in [16], [17]. It enables the use of state of the art phase retrieval algorithms that are now readily available and can be straightforwardly combined with any electromagnetic modeling tool.

Our main contribution is the numerical and experimental investigation of various measurement setups and phase retrieval algorithms. In addition to be computationally efficient, the presented approaches provide empirically good phase recovery performances with respect to noise, separation between scanning planes, and near field sampling step while providing an automatic setting of the initial guess.

The paper is organized as follows. The formulation of the phase retrieval problem and its resolution are described in Section II. Numerical investigations and experimental validations of the proposed near field phaseless measurement procedure for various radiating structures are shown in Sections III and IV. Conclusions are drawn in Section V.

II. Problem Formulation and Resolution

Our approach aims at computing appropriate equivalent sources that characterize the AUT from only phaseless near field measurements. The desired antenna radiation performances, including the far field pattern, can then be derived from these sources. Subsequently, the formulation of the problem through equivalent currents is described and its resolution using phase retrieval algorithms is detailed.

A. Formulation via Equivalent Currents

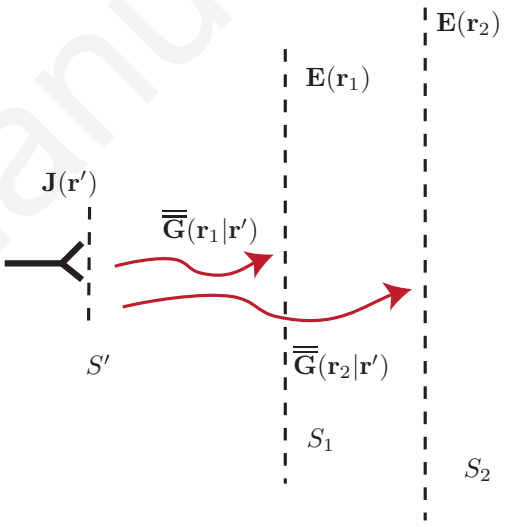

Fig. 1: Illustration of the phaseless near field antenna measurement problem.

The AUT can be represented by a set of equivalent currents by applying the equivalence principle of Schelkunoff [35]. We use the specific case of a planar Huygens surface and replace the semi-infinite space including the AUT by a perfect magnetic conductor. Therefore, the radiation of the AUT into the other semi-infinite space can be modelled by only electric equivalent currents, denoted $\mathbf{J}$, as explained on p.332 of [36]. The electric field at a position $\mathbf{r}$ on the measurement surface S can be therefore expressed as:

$$\mathbf{E}(\mathbf{r}) = \int_{S'} \overline{\overline{\mathbf{G}}}_{\mathrm{EJ}}(\mathbf{r}|\mathbf{r}') \cdot \mathbf{J}(\mathbf{r}')dS' \tag{2}$$

where $\overline{\overline{\mathbf{G}}}_{\mathrm{EJ}}$ is the electric field free space dyadic Green function for electric currents [36].

After discretization of the surface S', we define pulse basis functions to expand the unknown electric currents $\mathbf{J}(\mathbf{r}')$ and approximate the integral (2) using an appropriate quadrature

rule. The discretized version of the integral (2) can then be written as matrix equation:

$$\mathbf{e}(\mathbf{r}_i) = \mathbf{G}_{\mathrm{EJ}}(\mathbf{r}_i) \cdot \mathbf{j} \tag{3}$$

where $\mathbf{r}_i$ is a point on the surface S_i, with $i = \{1, 2\}$. The equation (3) is equivalent to:

$$\begin{bmatrix} \mathbf{e}_x(\mathbf{r}_i) \\ \mathbf{e}_y(\mathbf{r}_i) \\ \mathbf{e}_z(\mathbf{r}_i) \end{bmatrix} = \begin{bmatrix} \mathbf{G}_{EJ}^{(xx)}(\mathbf{r}_i) & \mathbf{G}_{EJ}^{(xy)}(\mathbf{r}_i) & \mathbf{G}_{EJ}^{(xz)}(\mathbf{r}_i) \\ \mathbf{G}_{EJ}^{(yx)}(\mathbf{r}_i) & \mathbf{G}_{EJ}^{(yy)}(\mathbf{r}_i) & \mathbf{G}_{EJ}^{(yz)}(\mathbf{r}_i) \\ \mathbf{G}_{EJ}^{(zx)}(\mathbf{r}_i) & \mathbf{G}_{EJ}^{(zy)}(\mathbf{r}_i) & \mathbf{G}_{EJ}^{(zz)}(\mathbf{r}_i) \end{bmatrix} \cdot \begin{bmatrix} \mathbf{j}_x \\ \mathbf{j}_y \\ \mathbf{j}_z \end{bmatrix} \tag{4}$$

We measure only the two components of the electric field that are tangential to the surfaces S_1 and S_2 (e.g. $\mathbf{e}_x(\mathbf{r}_i), \mathbf{e}_y(\mathbf{r}_i)$), and we reconstruct the electric equivalent currents that are tangential to the surface S' (e.g. $\mathbf{j}_x, \mathbf{j}_y$). Note, that in practice the radiation pattern of the probe has to be compensated [37]. When the near field phase is not available, a Phase Retrieval (PR) problem (1) has to be solved in order to reconstruct the complex equivalent currents $\mathbf{j}$. For that purpose, two near field scans (S_1 and S_2) are used to retrieve correctly these currents and mitigate the ambiguities. The PR problem amounts to find the equivalent currents $\mathbf{j}$ on S' that best fit the near field magnitudes $|\mathbf{e}(\mathbf{r}_1)|$ and $|\mathbf{e}(\mathbf{r}_2)|$ that are measured on the two scan surfaces S_1 and S_2, respectively. This PR problem can be formulated as:

$$\text{find } \mathbf{j} \quad \text{subject to} \quad \begin{cases} |\mathbf{e}(\mathbf{r}_1)| = |\mathbf{G}_{\mathrm{EJ}}(\mathbf{r}_1) \cdot \mathbf{j}| \\ |\mathbf{e}(\mathbf{r}_2)| = |\mathbf{G}_{\mathrm{EJ}}(\mathbf{r}_2) \cdot \mathbf{j}| \end{cases} \tag{5}$$

To ease the link between the standard PR formulation (1) and the problem at hand (5), let us specify:

- the near field magnitude vector: $\mathbf{y} = \begin{bmatrix} |\mathbf{e}(\mathbf{r}_1)| \\ |\mathbf{e}(\mathbf{r}_2)| \end{bmatrix}$,
- the sensing matrix: $\mathbf{A} = \begin{bmatrix} \mathbf{G}_{\mathrm{EJ}}(\mathbf{r}_1) \\ \mathbf{G}_{\mathrm{EJ}}(\mathbf{r}_2) \end{bmatrix}$
- the unknown current vector: $\mathbf{x} = \mathbf{j}$.

B. Resolution via Non-Convex Algorithms

Several PR approaches, reviewed in the introduction, have been proposed these last few years to solve (1). Among them, non-convex approaches solve a least-squares formulation of the PR problem [28], [30]–[32]. These methods apply a gradient descent to solve a problem of the form $\| |\mathbf{Ax}|^q - \mathbf{y}^q \|_2$, where the exponent $q = \{1, 2\}$. According to the approach, a subset of the measurements or a re-weighting version of the system $\mathbf{Ax} = \mathbf{y}$ is considered. These non-convex approaches can converge to the global optimum provided that they are seeded with a suitable initialization. Several smart initialization approaches have been advocated recently. The two main classes are spectral initializers [28] and its variants (truncated [29] and weighted [32] spectral initializers) and orthogonality promoting initializers [31]. The spectral method initializes $\mathbf{x}$ as the leading eigenvector of the matrix

$$\mathbf{S} = \frac{1}{m} \sum_{i=1}^{m} y_i \mathbf{a}_i \mathbf{a}_i^*$$

where $\mathbf{a}_i$ is the sampling vector and y_i is the observation. A truncated spectral version [29] discards the observations y_i that are several times larger than the mean to further improve the robustness of the original spectral initialization. The weighted spectral initializer boils down to finding a vector to maximize the weighted correlation with a subset $\mathcal{I}$ of selected sampling vectors $\mathbf{a}_i$. Details about its implementation are provided in [32]. On the contrary, the orthogonality promoting initializer works by identifying the vector that is most orthogonal to a subset of vectors $\{\mathbf{a}_i\}_{i \in \mathcal{I}}$, where $\mathcal{I}$ contains indices of the smallest measurements. This is achieved by forming the matrix:

$$\mathbf{S} = \frac{1}{|\mathcal{I}|} \sum_{i \in \mathcal{I}} \frac{\mathbf{a}_i \mathbf{a}_i^*}{\|\mathbf{a}_i\|^2}$$

where $|\mathcal{I}|$ is the cardinality of the set $\mathcal{I}$ and computing the eigenvector of $\mathbf{S}$ associated to the smallest eigenvalue.

We use the general purpose phase retrieval library PhasePack [33] that is a common software interface enabling to benchmark a large number of recent PR methods against one another, including the approaches and initializers described above.

III. Numerical Results

The PR procedure is assessed numerically by simulating with Ansys HFSS an array composed of 5 open-ended waveguides working at 30 GHz, represented in Fig. 2. These waveguides are fed by random complex excitations in order to radiate a *not too smooth* near field. The equivalent electric sources are placed on a plane of sampling step size 0.25λ above the waveguide apertures as represented in Fig. 2. This surface S' is at a height of $0.1\,\lambda$ above the waveguides and S' is larger than the radiating aperture by a factor of 1.5. The near field surfaces S_1 and S_2, represented in Fig. 2, are planes of dimension $20\lambda \times 10\lambda$. The influence of the heights of these planes and the sampling of the field on these planes are investigated.

The simulated complex near field on S_1 is considered as

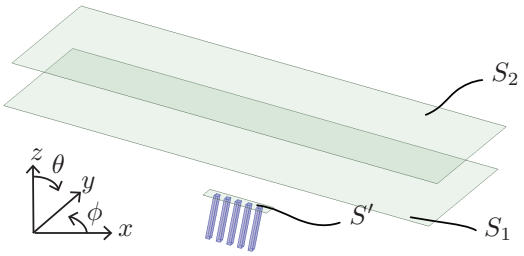

Fig. 2: 3D representation of the array of 5 waveguides with the equivalent current surface S' and the near field scanning surfaces S_1 and S_2.

the reference. To assess the PR procedure, we compare the field reconstructed from phaseless near field (by solving (5)) to this reference and compute the equivalent noise level (ENL) that measures the correlation between a pattern of reference $\mathbf{E}(\theta, \varphi)$ and an estimated one $\tilde{\mathbf{E}}(\theta, \varphi)$:

$$\mathrm{ENL} = 20 \log_{10} \left(\mathrm{mean} \left[\frac{|\mathbf{E}(\theta, \varphi) - \tilde{\mathbf{E}}(\theta, \varphi)|}{|\mathbf{E}(\theta, \varphi)_{\max}|} \right] \right).$$

A. PR Algorithms, Initializers and Near Field Sampling Step

We now compare the performances of 4 PR algorithms: Gerchberg-Saxton [18], Fienup [19], Reweighted Wirtinger Flow [30] and Reweighted Amplitude Flow [32]. For each of these 4 algorithms, we use 3 different initializers: a random complex vector for which the results are averaged over 20 iterations, a spectral initializer [28] and a weighted spectral initializer [31]. Note that the stopping criterion is a maximum number of iterations (set to 1000) unless a desired accuracy, quantified as the relative reconstruction error (set to 10^{-10}), is reached.
The far field of the reference, i.e. computed from the complex near field, is compared to the one reconstructed using the PR algorithms and the associated initializer. The results are plotted as a function of the regular near field sampling step 's' in Fig. 3. The spectral and weighted spectral initializers perform better than a random choice. Note that the standard Fienup and Gerchberg-Saxton algorithms perform fairly well with a random starting point. Other choices of initializers, such as orthogonal or truncated spectral, lead for this numerical example to recovery results similar to the spectral and weighted spectral initializers and have therefore been omitted. All 4 PR algorithms perform well for a near field sampling step $s \leq 0.5\lambda$. The Reweighted Amplitude Flow (RAF) with the weighted spectral initializer is the combination that yields the best PR reconstruction, very good recovery results (ENL around 50 dB) are achieved when $s \leq 0.5\lambda$ for this radiating structure.

B. Influence of the Noise

The measured near field is inevitably polluted by noise that can be modeled: $\mathbf{y}_n = |\mathbf{A}\mathbf{x} + \mathbf{n}|$, where the vector $\mathbf{n}$ is a complex Gaussian white noise. The level of the noise is quantified by the signal to noise ratio (SNR): $\text{SNR}_{\text{dB}} = 10\log_{10}(P_{\text{signal}}/P_{\text{noise}})$, where P_{signal} is the maximum measured power. We investigate the influence of the noise on the reconstruction using the 4 PR algorithms to estimate the robustness of these procedures. A near field sampling step of 0.5λ and a reweighted spectral initializer is chosen to perform this study since these settings provide good reconstruction results as previously shown.
The influence of the noise on the reconstruction of the PR reconstruction is plotted in Fig. 4. The reconstruction remains satisfactory with all 4 PR algorithms for a SNR above 40 dB. These performances are in general sufficient for anechoic chamber measurements. For instance, the SNR of our near field measurement setup has been estimated to about 100 dB.

C. Influence of Near Field Planes Heights

We investigate the influence of the distance between sampling planes, the plane S_1 is at a height of $2\,\lambda$ above the antenna aperture and the plane S_2 is at a height of $2\,\lambda + d$. A distance $d = 0$ means that only one measurement plane is considered. The same settings are kept: $s = 0.5\,\lambda$ and a weighted spectral initializer. The PR reconstruction results are plotted in Fig. 5. The RAF and RWF algorithms perform well from a distance $d = 1\,\lambda$ between the near field planes whereas the Fienup and Gerchberg-Saxton start to be efficient from $d \geq 2\,\lambda$.

TABLE I: Reconstruction performances of the standard gain horn

	Fienup	Gerchberg-Saxton	RWF	RAF
computation time ratio	8	8	1	1
ENL [dB]	-42.2	-42.2	-39.9	-44.7

D. Far Field Reconstruction

The RAF algorithm is applied to reconstruct the complex equivalent currents from phaseless measurements on S_1 and S_2 located at a height of 2 and $5\,\lambda$ respectively. A near field sampling step $s = 0.5\,\lambda$ is chosen. The ENL between the far field of reference (NF) and the reconstructed one (PR) is then equal to -49.2 dB. Considering the geometry of S_2 and S', the far field patterns can be correctly estimated for angles between $\pm 78^\circ$ and $\pm 66^\circ$ in the E- and H- planes, respectively. The total 3D far field patterns are shown in Fig. 6(a,b) whereas the co- and cross- polarizations of the field are plotted in Fig. 6(c,d). Discrepancies between the simulated and PR patterns are visible for low level field values (cross-polarization).
The computational time of the PR procedure is negligible with respect to the measurement time. For this example, it takes less than 1s to solve the PR problem (5) using the RAF algorithm on a biprocessor 2.79 GHz-CPU 64 GB-RAM Xeon. The Fienup and Gerchberg-Saxton algorithms are about 8 times slower.

IV. Experimental Validations

We use the RAF algorithm with a weighted spectral initializer to solve the PR problems for the following two antenna phaseless measurements.

A. Standard Gain Horn at 60 GHz

Equivalent electric currents are placed on the aperture of the horn with a step size of 0.25λ. They are the unknowns of the PR problem. The two near field surface scans S_1 and S_2 are squares of side 40λ located at heights of 5 and 13λ, which implies that the far field pattern can be correctly estimated for angles between $\pm 53^\circ$. The co-polarization of the near field is measured at 60 GHz with a sampling step s of 0.4λ.
The measured and reconstructed phase of the near fields are in good agreement as shown in Fig. 7. This is confirmed when looking at the far field patterns displayed in Fig. 8. The discrepancies at high angles with respect to the broadside direction ($\theta > 50^\circ$) are to be discarded because of the truncation of the near field plane. The performances and computation times of the four investigated algorithms are reported in Table I. Even if the RAF algorithm is the one leading to the best reconstruction results, the other PR algorithms also provide very satisfactory results. Note that the Fienup and Gerchberg-Saxton algorithms are 8 times slower than the RWF and RAF algorithms.

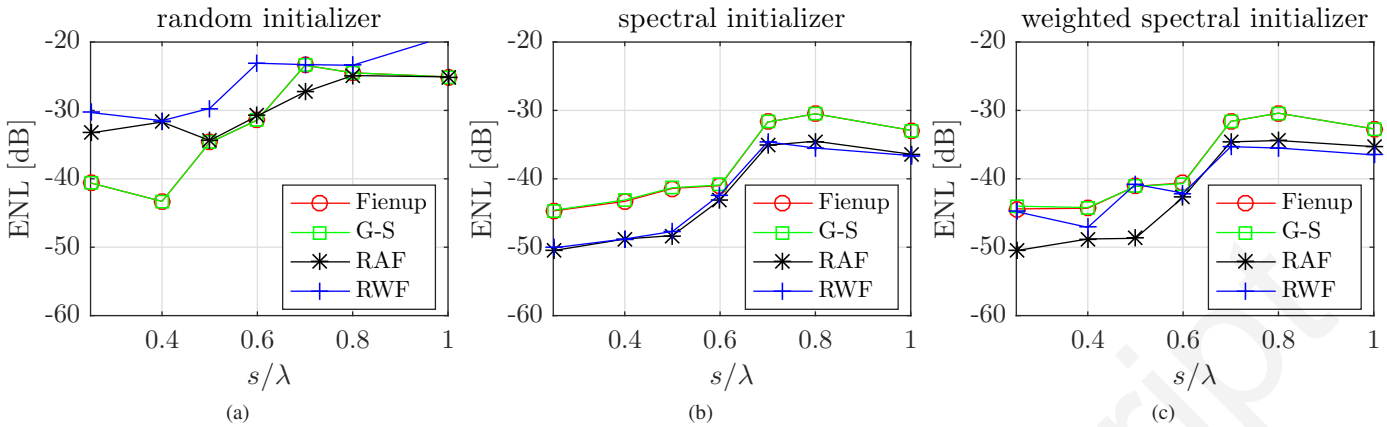

Fig. 3: Performances of 4 PR algorithms: Gerchberg-Saxton (G-S) [18], Fienup [19], Reweighted Wirtinger Flow (RWF) [30] and Reweighted Amplitude Flow (RAF) [32], for various initializers as a function of the near field sampling step s.

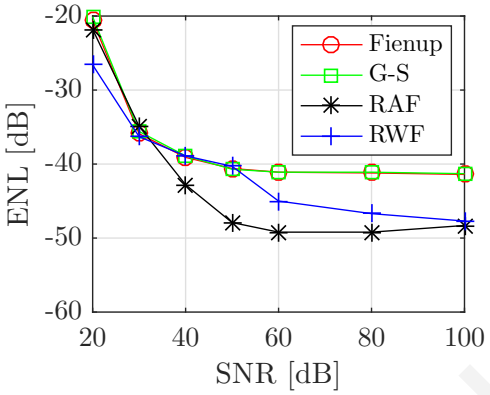

Fig. 4: Influence of the noise on the PR reconstruction of the waveguide array using 4 PR algorithms: Equivalent Noise Level (ENL) as a function of the SNR.

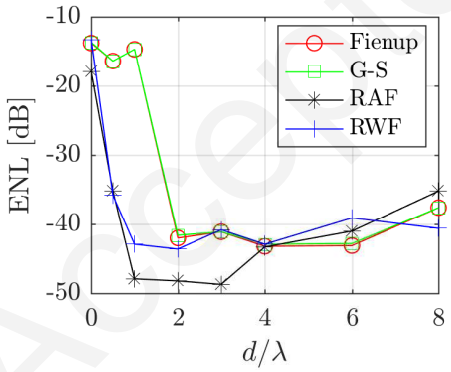

Fig. 5: Influence of the distance d between near field measurement planes on the far field reconstruction using 4 PR algorithms: Equivalent Noise Level (ENL) as a function of d. A distance d of $0\,\lambda$ means only one phaseless measurement plane is used.

B. Circularly Polarized Metasurface at 32 GHz

A metal-only metasurface has been designed to generate a circular polarization in Ka band. All details about the design and manufacturing of this radiating structure, shown in Fig. 9, are provided in [38]. Equivalent electric currents are placed above the metasurface with a step size of 0.25λ. The metasurface is measured at 32 GHz and the two near field surface scans S_1 and S_2 are squares of side 40λ located at heights of 5 and 13λ. Considering the geometry of S_2 and S', the far field patterns are expected to be accurately reconstructed for angles between $\pm 45^\circ$.

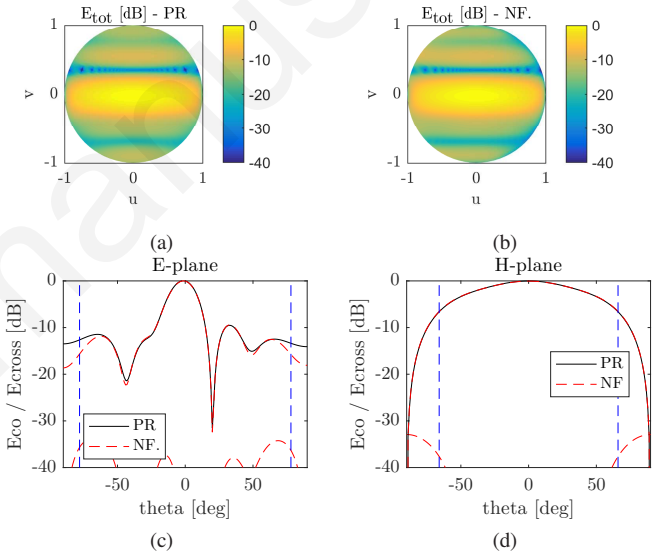

Fig. 6: 3D far field patterns of the array of 5 waveguides at 30 GHz derived from (a) the simulated complex near field (NF) and (b) the PR reconstructed near field. (c,d) show the corresponding patterns for both co- and cross- polarization of the field in the E- and H- planes, respectively. The vertical dashed lines define the range of validity of the reconstruction.

TABLE II: Reconstruction performances of the metasurface

	Fienup	Gerchberg-Saxton	RWF	RAF
computation time ratio	8.4	8.4	1.1	1
ENL [dB]	-24.7	-24.2	-41	-43.4

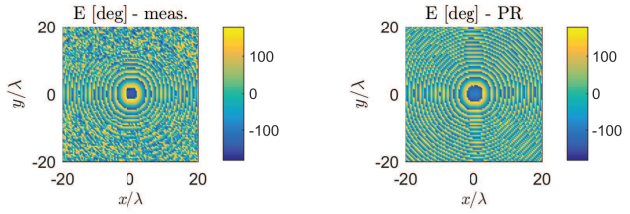

Fig. 7: Near field mappings at 60 GHz of the co-polarization of the field radiated by a standard gain horn at a height of 5λ. Phase of the near field (a) measured and (b) reconstructed by the PR procedure.

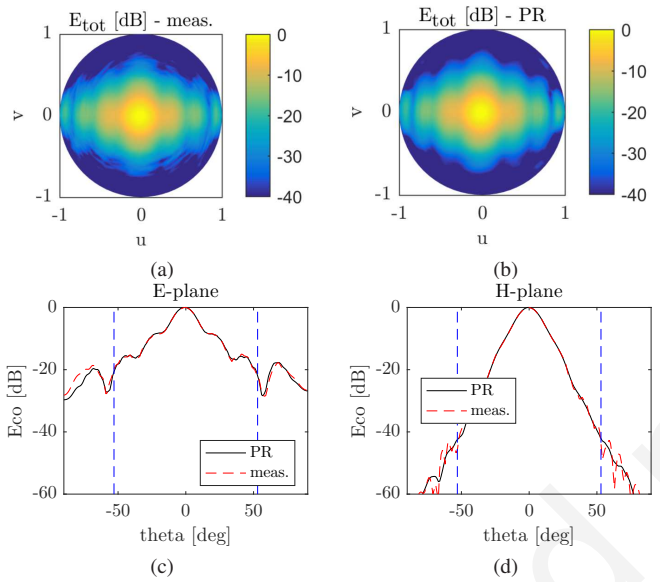

Fig. 8: 3D far field patterns of a standard gain horn at 60 GHz derived from (a) the measured near field and (b) the PR reconstructed near field. (c,d) show the corresponding patterns in the E- and H- plane respectively, where the vertical dashed lines define the range of validity of the reconstruction.

To assess the proposed PR procedure, we reconstruct the near field phase radiated by the metasurface from phaseless measurements and compare it to the measured complex near field. Note that the two components of the measured near field magnitude ($|\mathbf{e}_x|, |\mathbf{e}_y|$) must be considered at the same time to ensure that both components of the complex equivalent currents ($\mathbf{j}_x, \mathbf{j}_y$), and in particular their global phase difference, are properly reconstructed. The mappings of the near field phase are shown in Fig. 10. They are in very good agreement. To better estimate the quality of the field reconstruction from the phaseless measurements, we derive the far field and, more specifically, the right and left hand circular polarizations, denoted RHCP and LHCP respectively. A good agreement is obtained between the measured and reconstructed far field as shown in Fig. 11 and 12, which validates the proposed PR procedure. The performances and computation times of the four investigated algorithms are reported in Table II. The RWF and the RAF algorithms clearly lead to the best reconstruction

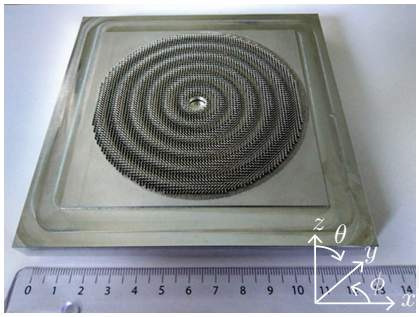

Fig. 9: Picture of the circularly polarized metasurface [38] of diameter 10λ at 32 GHz.

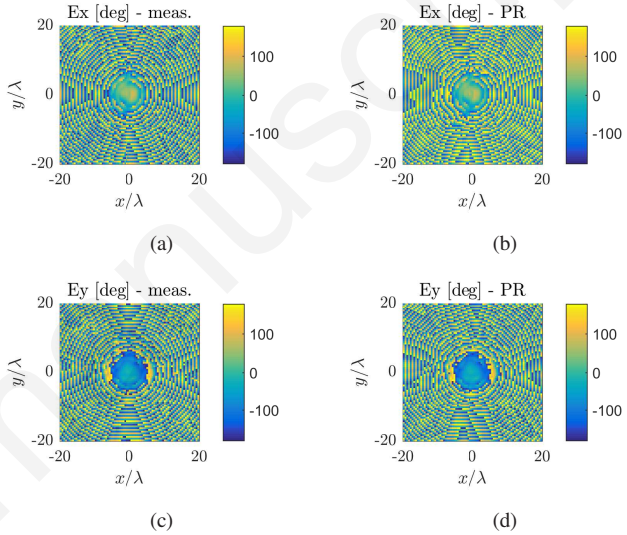

Fig. 10: Near field mappings at 32 GHz of the x- and y-component of the field radiated by the metasurface at a height of 5λ. Phase of the measured field (a,c) and the reconstructed one by the PR procedure (b,d).

results while being several order of magnitudes faster (of about a factor 8) than the Fienup and Gerchberg-Saxton algorithms.

V. Conclusion

The determination of antenna far-field pattern from near-field measurements has become an important part of modern antenna measurements for obvious practical reasons. It requires an accurate measurement of both amplitude and phase of the near field. However, the growing interest in submillimeter and terahertz frequency bands makes the acquisition of the phase cumbersome and expensive. Phaseless near field antenna measurements are then the only resort to properly characterize these antennas.

A procedure to determine the far field pattern, radiated by antennas from the measurement of two phaseless near field scans, has been proposed. It implies the resolution of a phase retrieval problem to compute the equivalent currents representing the antenna under test. Many phase retrieval algorithms have been proposed over the last decades and recent advances are discussed and compared in this paper. The latest tech-

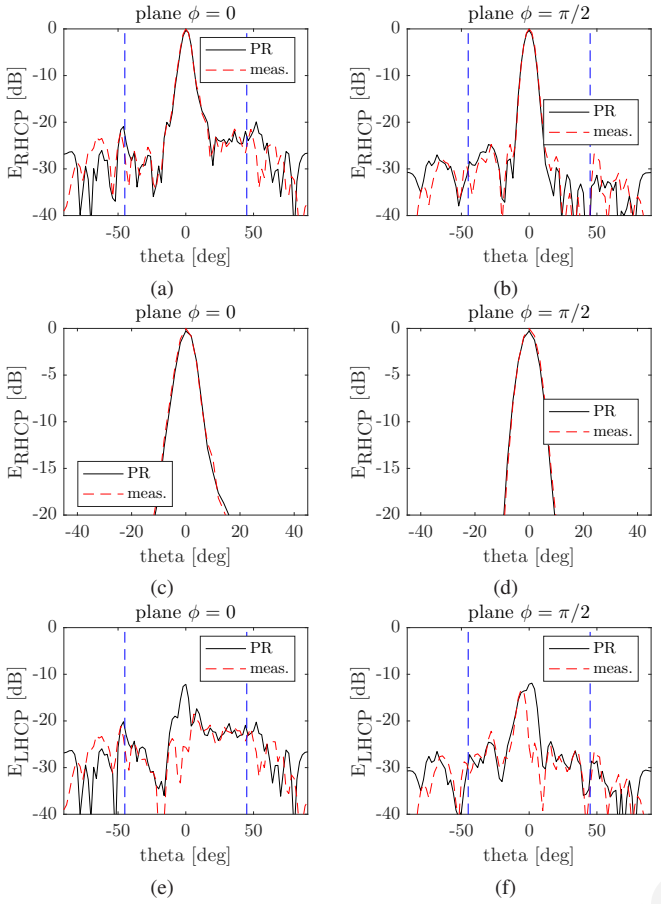

Fig. 11: 2D far field patterns (RHCP and LHCP) of the metasurface at 32 GHz derived from the measured near field and the phaseless near field. (a,b) show the RHCP component for the planes $\phi = 0$ and $\phi = \pi/2$, respectively. The patterns (c,d) are a zoom of the main beam of (a,b). (e,f) show the LHCP component for the planes $\phi = 0$ and $\phi = \pi/2$ respectively. The vertical dashed lines represent the limits of validity of the far field reconstruction.

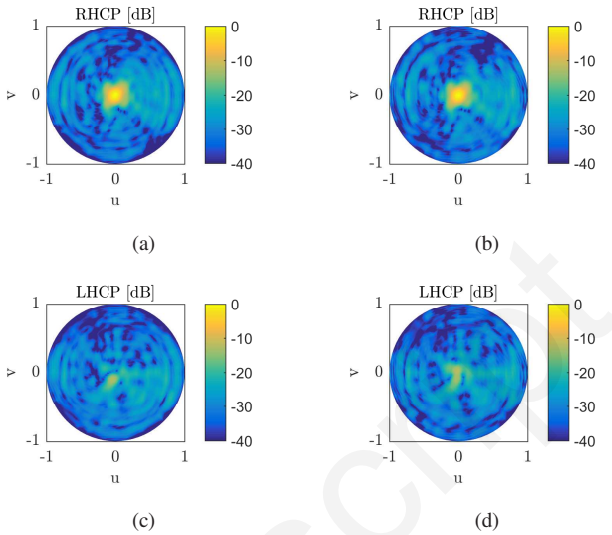

Fig. 12: 3D far field patterns (RHCP and LHCP) of the metasurface at 32 GHz derived from the measured near field (a,c) and the phaseless near field (b,d).

niques, that are computationally efficient and readily available, overcome a number of frequently encountered shortcomings and specifically the choice of the initial guess. Numerical investigations have been shown to demonstrate the robustness of the approach. The phaseless measurements of two radiating structures validate experimentally the proposed methodology.

References

[1] A.D. Yaghjian, "An overview of near-field antenna measurements," IEEE Trans. Antennas Propag., vol. 34, no. 1, pp. 30-45, Jan. 1986.

[2] S. Gregson, J. McCormick, and C. Parini, "Principles of Planar Near-Field Antenna Measurements," London, U.K.: IET, 2007.

[3] O. Breinbjerg, J. Fernandez Alvarez, "Phaseless Near-Field Antenna Measurement Techniques: An Overview," Proc. of 38th Annual Symposium of the Antenna Measurement Techniques Association, 2016.

[4] M.D. Migliore and G. Panariello, "A comparison among interferometric methods applied to array diagnosis from near-field data," in Proc. Inst. Elect. Eng. Microwaves Antennas and Propagation, vol. 148, pp. 261-267, Aug. 2001.

[5] S. Costanzo, G. Massa, and M. Migliore, "A novel hybrid approach for far-field characterization from near-field amplitude-only measurements on arbitrary scanning surfaces," IEEE Trans. Antennas. Propag., vol. 53, no. 6, pp. 1866-1874, June 2005.

[6] J. Laviada Martínez, A. Arboleya-Arboleya, Y. Álvarez-López, C. García-González, and F. Las-Heras, "Phaseless antenna diagnostics based on off-axis holography with synthetic reference wave," IEEE Antennas Wireless Propag. Lett., vol. 13, pp. 43-46, Jan. 2014.

[7] B. Fuchs and L. Le Coq, "Excitation retrieval of microwave linear arrays from phaseless far-field data," IEEE Trans. on Antennas and Propag., vol. 63, no. 2, pp. 748-754, 2015.

[8] O.M. Bucci, G. D'Elia, G. Leone, and R. Pierri, "Far-Field Pattern Determination from the Near-Field Amplitude on Two Surfaces," IEEE Trans. Antennas Propag., vol. 38, no. 11, pp. 1772-1779, May 1990.

[9] T. Isernia, G. Leone, and R. Pierri, "Radiation Pattern Evaluation from Near-field Intensities on Planes," IEEE Trans. Antennas Propag., vol. 44, no. 5, pp. 701-710, May 1996.

[10] T. Isernia, G. Leone, and R. Pierri, "Unique phase reconstruction of near fields over planes," Opt. Comm., vol. 130, no. 1-3, pp. 131-142, Sep. 1996.

[11] O.M. Bucci, G. D'Elia, and M.D. Migliore, "An effective near-field far-field transformation technique from truncated and inaccurate amplitude-only data," IEEE Trans. Antennas Propag. , vol. 47, no. 9, pp. 1377-1385, Sep. 1999.

[12] M.D. Migliore, F. Soldovieri, and R. Pierri, "Far-field antenna pattern estimation from near-field data using a low-cost amplitude-only measurement setup," IEEE Trans. Instrum. Meas., vol. 49, no. 1, pp. 71-76, Feb. 2000.

[13] R.G. Yaccarino and Y. Rahmat-Samii, "Phaseless Bi-Polar Planar Near-Field Measurements and Diagnostics of Array Antennas," IEEE Trans. on Antennas and Propag., vol. 47, no. 3, pp. 574-583, March 1999.

[14] S. Farhad Razavi and Y. Rahmat-Samii, "A new look at phaseless planar near-field measurements: limitations, simulations, measurements, and a hybrid solution," IEEE Antennas and Propagation Mag., vol. 49, no. 2, pp. 170-178, April 2007.

[15] A. Capozzoli, C. Curcio, G. D'Elia, and A. Liseno, "Phaseless Antenna Characterization by Effective Aperture Field and Data Representations," IEEE Trans. Antennas Propag., vol. 57, no. 1, pp. 215-230, Jan. 2009.

[16] F. Las-Heras and T.K. Sarkar, "A direct optimization approach for source reconstruction and NF-FF transformation using amplitude-only data," IEEE Trans. Antennas Propag., vol. 50, no. 4, pp. 500-510, Apr. 2002.

[17] Y. Alvarez, F. Las-Heras, and M.R. Pino, "The sources reconstruction method for amplitude-only measurements," IEEE Trans. Antennas Propag., vol. 58, no. 8, pp. 2776-2781, Aug. 2010.

[18] R. Gerchberg and W. Saxton, "A practical algorithm for the determination of phase from image and diffraction plane pictures," Optik, vol. 35, pp. 237-246, 1972.

[19] J. Fienup, "Phase retrieval algorithms: a comparison," Applied Optics, vol. 21, no. 15, pp. 2758-2769, 1982.

[20] E.J. Candès, Y.C. Eldar, T. Strohmer, and V. Voroninski. "Phase retrieval

via matrix completion," SIAM Rev., no. 57, vol. 2, pp.225-251, Nov. 2015.
[21] E.J. Candès, T. Strohmer, and V. Voroninski. "Phaselift : exact and stable signal recovery from magnitude measurements via convex programming," Commun. Pure Appl. Math., no. 66, vol. 8, pp. 1241-1274, 2013.
[22] I. Waldspurger, A. d'Aspremont, and S. Mallat, "Phase recovery, maxcut and complex semidefinite programming," Math. Program., vol. 149, no. 1-2, pp. 47-81, Feb. 2015.
[23] S. Bahmani and J. Romberg, "Phase retrieval meets statistical learning theory: A flexible convex relaxation," Intl. Conf. on Artificial Intelligence and Statistics (AISTATS), pp. 252-260, May 2017.
[24] T. Goldstein and C. Studer, "Convex phase retrieval without lifting," International Conference on Machine Learning, 2017.
[25] T. Goldstein and C. Studer, "PhaseMax: convex phase retrieval via basis pursuit," IEEE Trans. Inf. Theory, no. 64, vol. 4, pp. 2675-2689, April 2018.
[26] A. F. Morabito, R. Palmeri, V. A. Morabito, A. R. Laganà, and T. Isernia, "Single-Surface Phaseless Characterization of Antennas via Hierarchically Ordered Optimizations," IEEE Trans. Antennas Propag., vol. 67, no. 1, pp. 461-474, Jan. 2019.
[27] R. Ghods, A.S. Lan, T. Goldstein, and C. Studer, "Phaselin: Linear phase retrieval," 52nd Annual Conf. on Information Sciences and Systems (CISS), 2018.
[28] E.J. Candès, X. Li, and M. Soltanolkotabi "Phase retrieval via Wirtinger flow: Theory and algorithms," IEEE Trans. Inf. Theory, no. 61, vol. 4, pp. 1985-2007, Feb. 2015.
[29] Y. Chen and E.J. Candès, Solving random quadratic systems of equations is nearly as easy as solving linear systems, Comm. Pure Appl. Math., vol. 70, no. 5, pp. 822-883, Dec. 2017.
[30] Z. Yuan and H. Wang, "Phase retrieval via reweighted Wirtinger flow," Appl. Opt., vol. 56, no. 9, pp. 2418-2427, March 2017.
[31] G. Wang, G.B. Giannakis, and Y.C. Eldar, "Solving systems of random quadratic equations via truncated amplitude flow," IEEE Trans. Inf. Theory, vol. 64, no. 2, pp. 773-794, Feb. 2018.
[32] G. Wang, G.B. Giannakis, Y. Saad, J. Chen, "Phase Retrieval via Reweighted Amplitude Flow," IEEE Trans. Signal Proc., no. 66, vol. 11, pp. 2818-2833, June 2018.
[33] R. Chandra, C. Studer, and T. Goldstein. "Phasepack: A phase retrieval library," 51st Asilomar Conference on Signals, Systems, and Computers, 2017.
[34] A. Paulus, J. Knapp, and T.F. Eibert, "Phaseless Near-Field Far-Field Transformation Utilizing Combinations of Probe Signals," IEEE Trans. Antennas Propag., vol. 65, no. 10, pp. 5492-5502, Oct. 2017.
[35] S.A. Schelkunoff, "Some Equivalence Theorems of Electromagnetics and Their Application to Radiation Problems," Bell Syst. Tech. J. Vol. 15, pp. 92-112, 1936.
[36] C.A. Balanis, "Advanced Engineering in Electromagnetics," New York: Wiley, 1989.
[37] B. Joy, W.M. Leach Jr., G. P. Rodrigue, and D. T. Paris, "Application of probe-compensated near-field measurements," IEEE Trans. Antennas Propag., vol. 26, no. 3, pp. 379-389, May 1978.
[38] D. González-Ovejero, N.Chahat, R. Sauleau, G. Chattopadhyay, S. Maci and M. Ettorre, "Additive Manufactured Metal-Only Modulated Metasurface Antennas," IEEE Trans. Antennas Propag., vol. 66, no. 11, pp. 6106-6114, Nov. 2018.